Distinct Core Glycan and O-Glycoform Utilization of SARS-CoV-2 Omicron Variant Spike Protein RBD Revealed by Top-Down Mass Spectrometry

David S. Roberts,[1]* Morgan Mann,[2] Brad H. Li,[3] Donguk Kim,[4] Allan R. Brasier[2,5], Song Jin[1], Ying Ge[1,2,3]*

[1]Department of Chemistry, University of Wisconsin-Madison, Madison, WI 53706, USA.

[2]Department of Medicine, School of Medicine and Public Health, University of Wisconsin-Madison, Madison, WI 53705, USA.

[3] Department of Biochemistry, University of Wisconsin-Madison, WI 53706, USA.

[4] Department of Chemical and Biological Engineering, University of Wisconsin-Madison, WI 53706, USA.

[5]Institute for Clinical and Translational Research, University of Wisconsin-Madison, Madison, WI 53705, USA.

*Correspondence should be addressed to Y.G. (ying.ge@wisc.edu) and D.S.R. (dsroberts@wisc.edu)

Abstract

The SARS-CoV-2 Omicron (B.1.1.529) variant possesses numerous spike (S) mutations that enhance transmissibility and evasion of neutralizing antibodies, making it a serious threat to existing COVID-19 vaccines and therapies. Accurately distinguishing emerging S variants and revealing their post-translational glycosylation changes can provide new insights for rational design and development of vaccines and therapeutics. Here we report the first comprehensive elucidation of the molecular variations and O-glycoform changes of the Omicron, Delta (B.1.617.2), and wild-type (WA1/2020) S receptor-binding domains (S-RBDs) using high-resolution top-down mass spectrometry (MS). A novel O-glycosite (Thr376) unique to the Omicron variant is identified. Moreover, we have directly quantified the Core 1 and Core 2 O-glycan structures and characterized the O-glycoform structural heterogeneity of the three variants. Our findings provide high resolution detail of Omicron O-glycoform and utilization, providing new insights into how this variant escapes immunological protection and informing strategies for developing Omicron-directed vaccines and therapeutics.

Introduction

The rapid emergence of the new SARS-CoV-2 variants of concern (VOC) have destabilized global efforts to combat the novel 2019 coronavirus disease (COVID-19).[1] Although therapeutic antibodies and highly effective vaccines have led to significant progress in combatting COVID-19, the recent rise of more transmissible variants with mutations in the spike (S) protein threaten global efforts to control the pandemic.[2] New variants such as Delta (B.1.617.2) or Omicron (B.1.1.529) have been classified by the World Health Organization (WHO) as VOC due to their increased transmissibility, more severe disease, significant evasion of neutralizing antibodies from convalescents or vaccines, and their higher risk of eluding testing.[3] In particular, the Omicron variant possess an alarming number of mutations (>30), including 15 site mutations in the S receptor-binding domain (S-RBD) as compared to the wild-type (WT) strain (WA1/2020), making it of particular concern given that the S-RBD is the principal target for neutralizing antibodies and other therapeutics.[4] Recent clinical data for the highly mutated Omicron variant has already been demonstrated to cause higher rates of reinfection and rampant breakthrough infections despite mRNA vaccine booster dose.[5]

Furthermore, S protein glycosylation is critically involved in human receptor ACE2 binding,[6] cell infectivity,[7] and shields epitopes from antibody neutralization.[8] Although S protein N-glycosylation has been characterized in detail[9] with ongoing efforts to understand the impact of N-glycosylation for vaccine development,[10] characterization of O-glycosylation is challenging[11] due to the large microheterogeneity and structural diversity of O-glycans leading to multiple O-glycoforms.[12] To address these challenges we have recently developed a hybrid top-down mass spectrometry (MS) approach[13] that is capable of simultaneous characterization of the molecular

structures, the site specificity, and the relative abundance of various glycoforms along with the overall post-translational modification (PTM) compositions of different coappearing 'proteoforms'[14] to enable proteoform-resolved analysis[15] of complex glycoproteins. Given the rapid mutation and spread of emerging SARS-CoV-2 variants, there is an urgent need for accurately distinguishing S variants and elucidating their post-translational glycosylation changes to provide new avenues for rational therapeutic development.

Here we report the first comprehensive analysis of the sites and O-glycoform structures of the Delta and Omicron SARS-CoV-2 variants by top-down MS. Not only has a new O-glycan site been observed, but also top-down O-glycoform quantification revealed significant enhancement of Core 2 type O-glycan structures for Omicron, as compared to the WT or Delta variants.

Results and Discussion

The mutational differences inherent to the Delta and Omicron variants, as compared to the WT strain, are especially pronounced in their RBDs (Figure 1A). To elucidate the molecular sequence and O-glycans of the various S-RBDs, we completely removed the N-glycans from the S-RBD using a PNGase F treatment (see Supporting Information)[13] to minimize the interference posed by N-glycan heterogeneity (Figure 1B). The removal of N-glycans yielded a >10 kDa of molecular weight loss compared to the fully glycosylated S-RBD. The resulting S-RBD O-glycoforms were resolved by an ultrahigh resolution 12 T Fourier transform ion cyclotron (FTICR)-MS (Figure 1C). Impressively, baseline isotopic resolution was achieved for the various S-RBD owing to the high resolving power of the FTICR-MS (Figures S1-S3). Top-down MS analysis revealed significant differences in the stoichiometry and relative abundance of various O-

glycoforms, with the Omicron variant showing the greatest O-glycoform structural heterogeneity (Figure 1C).

To achieve in-depth glycoform and glycosite analysis, we utilized trapped ion mobility spectrometry (TIMS)-MS to separate and analyze the various S-RBD O-glycan structures via a timsTOF Pro instrument following the N-glycan removal (Figure 2). To characterize the glycan structures and occupancy of the highly mutated Omicron variant, we performed specific isolation of the individual S-RBD O-glycoforms. Focusing on the most abundant O-glycoform (26+ charge state, 1069.4.3 *m/z*) as a specific example, MS/MS fragment ions obtained from collisionally activated dissociation (CAD) were output from the Bruker DataAnalysis software and analyzed in targeted protein analysis mode using MASH Explorer[16] for comprehensive proteoform characterization. The top-down MS/MS spectra were obtained along with ion mobility separation of the various O-glycan structures to overcome the mass degeneracy and microheterogeneity inherent to O-glycans analysis (Figure 2B). Sufficiently soft TIMS cell activation parameters enabled detailed neutral loss mapping of the isolated S-RBD proteoform and revealed a Core 1 (Galβ1-3GalNAc-Ser/Thr) O-glycan with a GalNAcGal$(NeuAc)_2$ structure (Figure 2C). This TIMS-MS approach allowed for the direct characterization of the glycan structures to reveal multiple S-RBD glycoforms with Core 1 and Core 2 (GlcNAcβ1-6(Galβ1-3)GalNAc-Ser/Thr) O-glycan structures across the three S-RBD variants (Figure S4).

We then further characterized the S-RBD WT, Delta, and Omicron O-glycosylation patterns to reveal all the structural O-glycoform alterations between the variants (Figure 3). Interestingly, we observed major O-glycan microheterogeneity changes in Omicron as compared to the WT or Delta variants. In particular, we found significantly enhanced Core 2 O-glycan

structure abundances for Omicron with pronounced expression for multiply sialylated GalNAc(GalNeuAc)(GlcNAcGalNeuAc) and fucosylated GalNAc(GalNeuAc)(GlcNAcGalFuc) structures. The striking molecular abundance differences observed in Omicron as compared to the WT or Delta variants are summarized in Table 1.

Table 1. Summary of the S-RBD variants O-glycoform relative abundances.

O-glycoform structure	Cr.[a]	WT (%)	Delta (%)	Omicron (%)
GalNAcGalNeuAc	1	1.3	1.4	2.3
GalNAcGal(NeuAc)$_2$	1	80.9	86.2	69.0
GalNAc(GalNeuAc)(GlcNAcGal)[b]	2	5.8	3.8	5.4
GalNAc(GalNeuAc)(GlcNAcGalFuc)[b]	2	5.2	3.2	13.2
GalNAc(GalNeuAc)(GlcNAcGalNeuAc)	2	6.8	5.3	10.0

[a] O-glycan core type. [b] Combined abundance including O-glycoforms with a N-terminal acetylation (WT, Delta) or N-terminal trimethylation (Omicron).

The relative abundance of Core 1 to Core 2 S-RBD O-glycan structures for the Omicron variant was roughly 71:29, with the Core 1 GalNAcGal(NeuAc)$_2$ being the most abundant O-glycoform (~69% relative abundance). Interestingly, the WT and Delta variants show a strong bias toward Core 1 type O-glycan structures, with more than 80% of its O-glycoform abundance corresponding to the Core 1 GalNAcGal(NeuAc)$_2$ structure. The Omicron variant was found to possess a Core 2 type GalNAc(GalNeuAc)(GlcNAcGalFuc) structure that accounts for more than 13% of its total O-glycoform composition (Figures 3 and S5). Moreover, we characterized the abundant (10 %) Core 2 GalNAc(GalNeuAc)(GlcNAcGalNeuAc) structure for the Omicron variant (Figures 3 and S6). These particular Core 2 structures were also found in the WT and Delta S-RBD variants but at much lower (5-7%) relative abundances. The high-resolution intact S-RBD glycoform characterization shown in Figure 3 demonstrates the distinct advantages of this top-down MS approach over glycopeptide-based bottom-up MS approaches.[17]

We then further investigated the glycosites and their microheterogeneity between the S-RBD variants. Figure 4 shows a specific example of top-down MS/MS O-glycosite determination using the highly abundant Core 1 GalNAcGal(NeuAc)$_2$ structure. Detailed top-down MS/MS analysis of the S-RBD O-glycoforms revealed the presence of a new O-glycosite (Thr376) unique to the Omicron variant (Figure 4A). Fascinatingly, all detected S-RBD O-glycans for the WT and Delta variants were confidently assigned solely to Thr323 (Figures 4B and 4C), which agrees with previous studies on WT S O-glycosylation.[18] Representative CAD fragment ions for the WT (b_7^{1+} and b_{173}^{11+}) and Delta (b_7^{1+} and b_{233}^{12}) confidently localized the O-glycosite to Thr323 (Figures 4b-c and S7). Given the smaller number of mutations present on Delta as compared to Omicron, it is not surprising that the O-glcyosite Thr323 was conserved between Delta and WT variants. On the other hand, the Omicron variant yielded both the familiar Thr323 O-glycosite (b_5^{1+} and b_{18}^{2+}) and a new Thr376 O-glycosite (b_{60}^{12+} and b_{52}^{5+}) corresponding to the GalNAcGal(NeuAc)$_2$ O-glycoform (Figure 4D). This Thr376 O-glycosite is conveniently n + 3 adjacent to a proline at residue 373, which is consistent with previous reports of increased O-glycosylation frequency near proline.[19] This particular Pro373 is a site-specific mutation unique to the Omicron variant and likely is the reason for this new O-glycosite. We note that the occupancy of the Thr376 site is low relative to the T323 (< 30%) and was only confidently assigned for the abundant GalNAcGal(NeuAc)$_2$ O-glycoform, although we suspect other Core 2 O-glycoforms may also possess the Thr376 modification. Moreover, although the assigned O-glycoforms for the variants are specific to S-RBD expressed from HEK293 cells, the HEK293 expression model is known to reflect the glycosylation sites expected for the viron.[20]

Conclusion

In summary, we report the first comprehensive molecular elucidation of the O-glycoform structural heterogeneity found in SARS-CoV-2 Omicron and Delta variants. We observed significant enhancement in the utilization of Core 2 type O-glycoforms for the Omicron variant as compared to WT or Delta. Moreover, we identified and characterized a novel Thr376 O-glycosite unique to Omicron S-RBD. This top-down MS approach is complimentary to traditional structural methods such as X-ray crystallography and cryoEM, which are not amenable for direct glycan structural analysis due to the inherent flexibility and heterogeneity of oligosaccharides,[21] and provides unmatched resolution for the characterization of SARS-CoV-2 S-RBD proteoforms. Importantly, this top-down MS approach establishes a necessary molecular foundation to understand the structure-function significance of S mutations and PTM changes in emerging SARS-CoV-2 variants. Our findings may provide new insights into how Omicron escapes immunological protection and can inform strategies for developing new variant-directed vaccines and therapeutics.

Acknowledgement

This research is supported by NIH R01 GM117058 (to S.J. and Y.G.). Y.G. would like to acknowledge NIH R01 GM125085, R01 HL096971, and S10 OD018475. D.S.R. also acknowledges the support from the American Heart Association Predoctoral Fellowship Grant No. 832615/David S. Roberts/2021. We also thank Michael Greig, Guillaume Tremintin, Conor Mullins, Gary Kruppa, Paul Speir, and Rohan Thakur of Bruker Daltonics for their helpful discussion and provision of the Bruker timsTOF Pro used in this work.

Notes

The authors declare no competing financial interest.

Figures

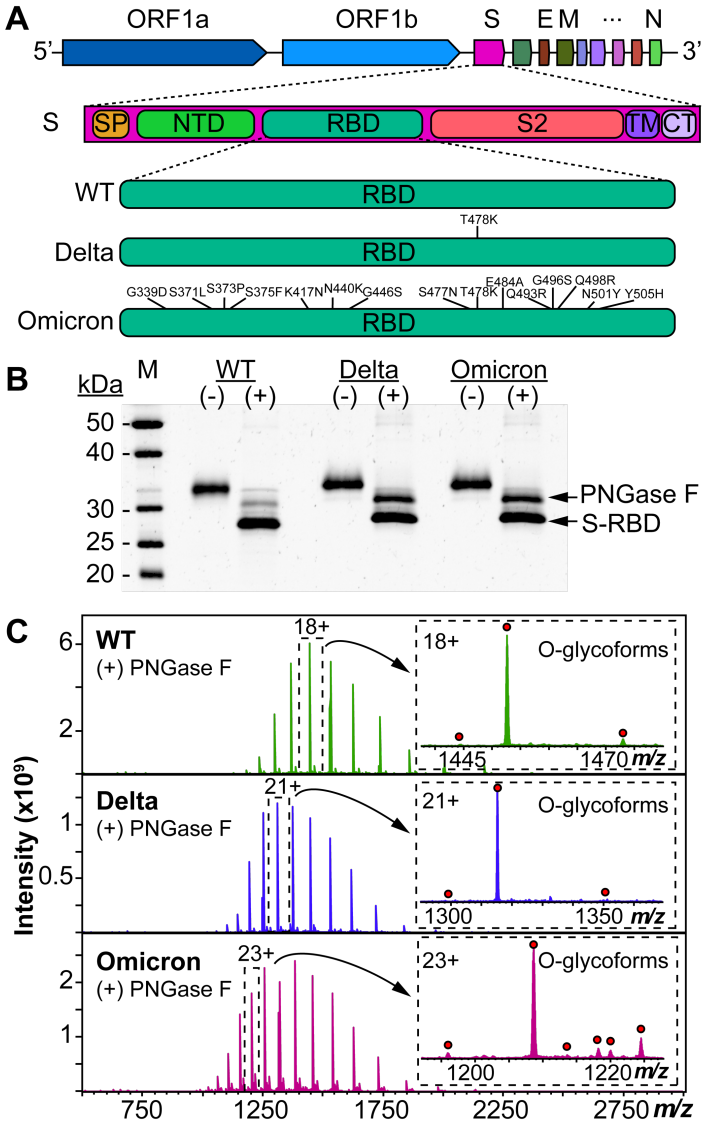

Figure 1. Protein mutational mapping and high-resolution top-down MS of S-RBD arising from the WT, Delta, and Omicron variants. (A) Architecture of SARS-CoV-2 genome and illustration of the protein sequence changes for the S-RBD variants. (B) SDS-PAGE of the S-RBD variants before (−) and after (+) PNGase F treatment. Gel lanes were equally loaded (300 ng), and gel staining was visualized by SYPRO Ruby. (C) Raw MS^1 of intact S-RBD proteoforms after PNGase F treatment for the WT, Delta, and Omicron variants. All identified O-glycoforms are annotated in the inset with a red circle.

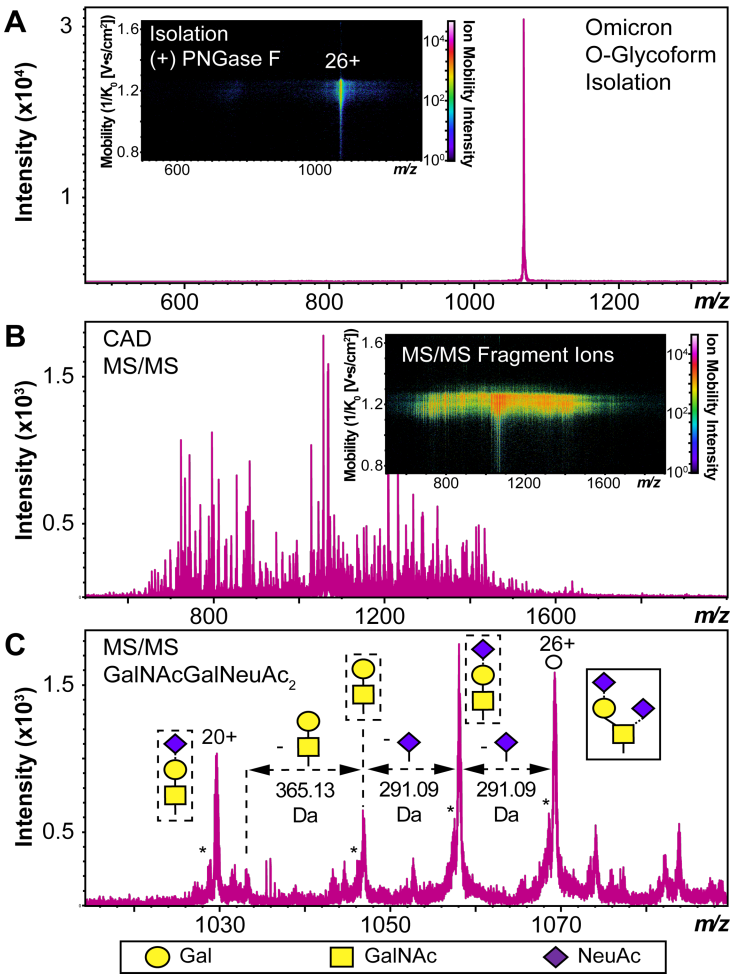

Figure 2. S-RBD O-glycoform analysis by TIMS-MS. (A) Illustration of the isolation of a specific Omicron S-RBD glycoform (z = 26+, centered at 1069.4 m/z) after PNGase F treatment using TIMS-MS. (Inset) Associated ion mobility heat map after isolation of the precursor. (B) Top-down MS/MS of Omicron S-RBD O-glycoform following CAD fragmentation of the isolated proteoform. A collision cell voltage of 22 eV was applied for this specific example. (C) Neutral loss O-glycan mapping of the Omicron S-RBD proteoform. Glycoform characterization reveals the specific S-RBD proteoform to have a Core 1 type $GalNAcGalNeuAc_2$ glycan structure. Assignments of the glycan structures are marked in the spectrum with the legend shown on the bottom. The hollow circle represents the 26+ charge state precursor ion corresponding to the 1069.4 m/z isolation. An asterisk "*" denotes an oxonium ion loss.

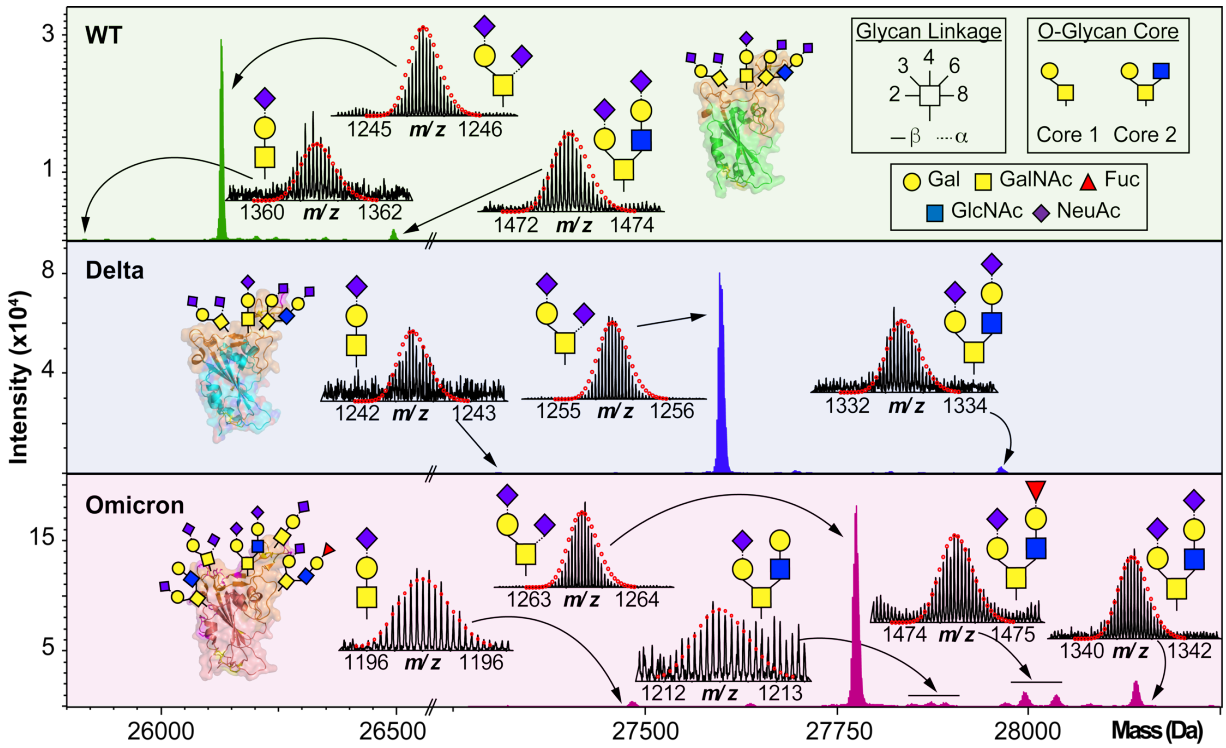

Figure 3. O-glycoform characterization of the S-RBD variants. Deconvoluted MS of the S-RBD proteoforms are shown with all major O-glycan assignments for the WT (green), Delta (blue), and Omicron (pink) variants. Insets show the isotopically and baseline resolved S-RBD proteoform MS spectra allowing for accurate determination of individual intact glycoforms. All individual ion assignments are within 1 ppm from the theoretical mass and theoretical isotopic distributions are indicated by the red dots. Assignments of the glycan structures are marked in the spectrum with the legend shown as an inset. PDB: 6M0J, 7WBQ, 7WBP.

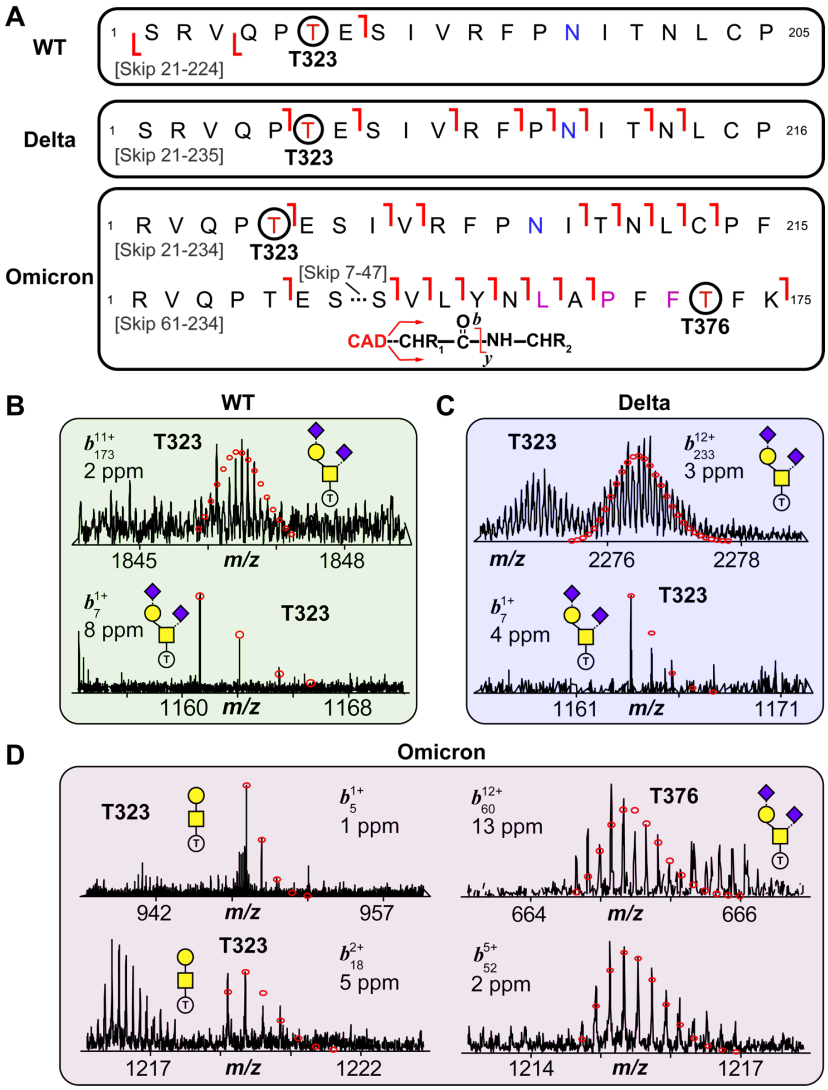

Figure 4. S-RBD O-glycosite localization by top-down MS/MS. (A) Fragmentation mapping of the Core 1 type GalNAcGal(NeuAc)$_2$ glycan corresponding to the WT, Delta, and Omicron S-RBD variants. Amino acid sequence (Arg319-Phe541) was based on the entry name P0DTC2 (SPIKE_SARS2) obtained from the UniProtKB sequence database with appropriate amino acid substitutions made for the mutated Delta and Omicron variants. Cleavage of signal peptide tPA following cell expression results in the N-terminal Ser for the WT and Delta variants. The blue N (Asn) denotes deamidation following PNGase F treatment. Specific Omicron residue mutations are denoted with a pink residue. (B-D) Representative top-down MS/MS CAD fragment ions of intact WT (b_7^{1+} and b_{173}^{11+}) (B), Delta (b_7^{1+} and b_{223}^{12+}) (C), and Omicron (b_5^{1+}, b_{18}^{2+}, b_7^{1+}, b_{173}^{11+}) (D) variants corresponding to the GalNAcGal(NeuAc)$_2$ O-glycoform shown in (A). WT and Delta variants showed complete O-glycosite occupation at Thr323. The Omicron variant was found to possess both Thr323 (left side; $b_5^{1+}$and b_{18}^{2+}) and Thr376 (right side; b_7^{1+}, and b_{173}^{11+}) as O-glycosites corresponding to the same Core 1 O-glycan structure. Theoretical isotopic distributions are indicated by the red dots and mass accuracy errors are listed for each fragment ion.

References

(1) VanBlargan, L. A.; Errico, J. M.; Halfmann, P. J.; Zost, S. J.; Crowe, J. E.; Purcell, L. A.; Kawaoka, Y.; Corti, D.; Fremont, D. H.; Diamond, M. S. An infectious SARS-CoV-2 B.1.1.529 Omicron virus escapes neutralization by therapeutic monoclonal antibodies. *Nature Medicine* **2022**. DOI: 10.1038/s41591-021-01678-y.
(2) Viana, R.; Moyo, S.; Amoako, D. G.; Tegally, H.; Scheepers, C.; Althaus, C. L.; Anyaneji, U. J.; Bester, P. A.; Boni, M. F.; Chand, M.; et al. Rapid epidemic expansion of the SARS-CoV-2 Omicron variant in southern Africa. *Nature* **2022**. DOI: 10.1038/s41586-022-04411-y.
(3) Morens, D. M.; Taubenberger, J. K.; Fauci, A. S. Universal Coronavirus Vaccines — An Urgent Need. *New England Journal of Medicine* **2021**, *386* (4), 297-299. DOI: 10.1056/NEJMp2118468 (acccessed 2022/02/03).
(4) Liu, L.; Iketani, S.; Guo, Y.; Chan, J. F. W.; Wang, M.; Liu, L.; Luo, Y.; Chu, H.; Huang, Y.; Nair, M. S.; et al. Striking Antibody Evasion Manifested by the Omicron Variant of SARS-CoV-2. *Nature* **2021**. DOI: 10.1038/s41586-021-04388-0. Shin, Y.-H.; Jeong, K.; Lee, J.; Lee, H. J.; Yim, J.; Kim, J.; Kim, S.; Park, S. B. Inhibition of ACE2-Spike Interaction by an ACE2 Binder Suppresses SARS-CoV-2 Entry. *Angewandte Chemie International Edition* **2022**, *n/a* (n/a), e202115695, https://doi.org/10.1002/anie.202115695. DOI: https://doi.org/10.1002/anie.202115695 (acccessed 2022/02/04).
(5) Kuhlmann, C.; Mayer, C. K.; Claassen, M.; Maponga, T.; Burgers, W. A.; Keeton, R.; Riou, C.; Sutherland, A. D.; Suliman, T.; Shaw, M. L.; et al. Breakthrough infections with SARS-CoV-2 omicron despite mRNA vaccine booster dose. *The Lancet* **2022**. DOI: 10.1016/S0140-6736(22)00090-3 (acccessed 2022/02/03).
(6) Casalino, L.; Gaieb, Z.; Goldsmith, J. A.; Hjorth, C. K.; Dommer, A. C.; Harbison, A. M.; Fogarty, C. A.; Barros, E. P.; Taylor, B. C.; McLellan, J. S.; et al. Beyond Shielding: The Roles of Glycans in the SARS-CoV-2 Spike Protein. *ACS Central Science* **2020**, *6* (10), 1722-1734. DOI: 10.1021/acscentsci.0c01056.
(7) Zhang, L.; Mann, M.; Syed, Z. A.; Reynolds, H. M.; Tian, E.; Samara, N. L.; Zeldin, D. C.; Tabak, L. A.; Ten Hagen, K. G. Furin cleavage of the SARS-CoV-2 spike is modulated by O-glycosylation. *Proceedings of the National Academy of Sciences* **2021**, *118* (47), e2109905118. DOI: 10.1073/pnas.2109905118.
(8) Harvey, W. T.; Carabelli, A. M.; Jackson, B.; Gupta, R. K.; Thomson, E. C.; Harrison, E. M.; Ludden, C.; Reeve, R.; Rambaut, A.; Peacock, S. J.; et al. SARS-CoV-2 variants, spike mutations and immune escape. *Nature Reviews Microbiology* **2021**, *19* (7), 409-424. DOI: 10.1038/s41579-021-00573-0.
(9) Lenza, M. P.; Oyenarte, I.; Diercks, T.; Quintana, J. I.; Gimeno, A.; Coelho, H.; Diniz, A.; Peccati, F.; Delgado, S.; Bosch, A.; et al. Structural Characterization of N-Linked Glycans in the Receptor Binding Domain of the SARS-CoV-2 Spike Protein and their Interactions with Human Lectins. *Angewandte Chemie International Edition* **2020**, *59* (52), 23763-23771, https://doi.org/10.1002/anie.202011015. DOI: https://doi.org/10.1002/anie.202011015 (acccessed 2021/03/08). Watanabe, Y.; Allen, J. D.; Wrapp, D.; McLellan, J. S.; Crispin, M. Site-specific glycan analysis of the SARS-CoV-2 spike. *Science* **2020**, eabb9983. DOI: 10.1126/science.abb9983.
(10) Huang, H.-Y.; Liao, H.-Y.; Chen, X.; Wang, S.-W.; Cheng, C.-W.; Shahed-Al-Mahmud, M.; Chen, T.-H.; Lo, J. M.; Liu, Y.-M.; Wu, Y.-M.; et al. Impact of glycosylation on a broad-spectrum vaccine against SARS-CoV-2. *bioRxiv* **2021**, 2021.2005.2025.445523. DOI: 10.1101/2021.05.25.445523.
(11) Rangel-Angarita, V.; Malaker, S. A. Mucinomics as the Next Frontier of Mass Spectrometry. *ACS Chemical Biology* **2021**, *16* (10), 1866-1883. DOI: 10.1021/acschembio.1c00384. Escobar, E. E.; King, D. T.; Serrano-Negrón, J. E.; Alteen, M. G.; Vocadlo, D. J.; Brodbelt, J. S. Precision Mapping of O-Linked N-Acetylglucosamine Sites in Proteins Using Ultraviolet Photodissociation Mass Spectrometry. *Journal of the American Chemical Society* **2020**, *142* (26), 11569-11577. DOI: 10.1021/jacs.0c04710.

(12) Jensen, P. H.; Kolarich, D.; Packer, N. H. Mucin-type O-glycosylation – putting the pieces together. *The FEBS Journal* **2010**, *277* (1), 81-94, https://doi.org/10.1111/j.1742-4658.2009.07429.x. DOI: https://doi.org/10.1111/j.1742-4658.2009.07429.x (acccessed 2020/11/10). Riley, N. M.; Bertozzi, C. R.; Pitteri, S. J. A Pragmatic Guide to Enrichment Strategies for Mass Spectrometry–Based Glycoproteomics. *Molecular & Cellular Proteomics* **2021**, *20*, 100029. DOI: https://doi.org/10.1074/mcp.R120.002277.
(13) Roberts, D. S.; Mann, M.; Melby, J. A.; Larson, E. J.; Zhu, Y.; Brasier, A. R.; Jin, S.; Ge, Y. Structural O-Glycoform Heterogeneity of the SARS-CoV-2 Spike Protein Receptor-Binding Domain Revealed by Top-Down Mass Spectrometry. *Journal of the American Chemical Society* **2021**, *143* (31), 12014-12024. DOI: 10.1021/jacs.1c02713.
(14) Smith, L. M.; Kelleher, N. L.; The Consortium for Top Down, P.; Linial, M.; Goodlett, D.; Langridge-Smith, P.; Ah Goo, Y.; Safford, G.; Bonilla*, L.; Kruppa, G.; et al. Proteoform: a single term describing protein complexity. *Nature Methods* **2013**, *10*, 186, Correspondence. DOI: 10.1038/nmeth.2369

https://www.nature.com/articles/nmeth.2369#supplementary-information.
(15) Tiambeng, T. N.; Roberts, D. S.; Brown, K. A.; Zhu, Y.; Chen, B.; Wu, Z.; Mitchell, S. D.; Guardado-Alvarez, T. M.; Jin, S.; Ge, Y. Nanoproteomics enables proteoform-resolved analysis of low-abundance proteins in human serum. *Nature Communications* **2020**, *11* (1), 3903. DOI: 10.1038/s41467-020-17643-1. Brown, K. A.; Melby, J. A.; Roberts, D. S.; Ge, Y. Top-down proteomics: challenges, innovations, and applications in basic and clinical research. *Expert Review of Proteomics* **2020**, *17* (10), 719-733. DOI: 10.1080/14789450.2020.1855982.
(16) Wu, Z.; Roberts, D. S.; Melby, J. A.; Wenger, K.; Wetzel, M.; Gu, Y.; Ramanathan, S. G.; Bayne, E. F.; Liu, X.; Sun, R.; et al. MASH Explorer: A Universal Software Environment for Top-Down Proteomics. *Journal of Proteome Research* **2020**, *19* (9), 3867-3876. DOI: 10.1021/acs.jproteome.0c00469.
(17) Yen, H.-Y.; Liko, I.; Gault, J.; Wu, D.; Struwe, W. B.; Robinson, C. V. Correlating Glycoforms of DC-SIGN with Stability Using a Combination of Enzymatic Digestion and Ion Mobility Mass Spectrometry. *Angewandte Chemie International Edition* **2020**, *59* (36), 15560-15564, https://doi.org/10.1002/anie.202005727. DOI: https://doi.org/10.1002/anie.202005727 (acccessed 2021/02/16). Melby, J. A.; Roberts, D. S.; Larson, E. J.; Brown, K. A.; Bayne, E. F.; Jin, S.; Ge, Y. Novel Strategies to Address the Challenges in Top-Down Proteomics. *Journal of the American Society for Mass Spectrometry* **2021**, *32* (6), 1278-1294. DOI: 10.1021/jasms.1c00099.
(18) Shajahan, A.; Supekar, N. T.; Gleinich, A. S.; Azadi, P. Deducing the N- and O-glycosylation profile of the spike protein of novel coronavirus SARS-CoV-2. *Glycobiology* **2020**. DOI: 10.1093/glycob/cwaa042 (acccessed 8/31/2020).
(19) Hema Thanka Christlet, T.; Veluraja, K. Database Analysis of O-Glycosylation Sites in Proteins. *Biophysical Journal* **2001**, *80* (2), 952-960. DOI: https://doi.org/10.1016/S0006-3495(01)76074-2.
(20) Bagdonaite, I.; Wandall, H. H. Global aspects of viral glycosylation. *Glycobiology* **2018**, *28* (7), 443-467. DOI: 10.1093/glycob/cwy021 (acccessed 4/13/2020). Breidenbach, J.; Lemke, C.; Pillaiyar, T.; Schäkel, L.; Al Hamwi, G.; Diett, M.; Gedschold, R.; Geiger, N.; Lopez, V.; Mirza, S.; et al. Targeting the Main Protease of SARS-CoV-2: From the Establishment of High Throughput Screening to the Design of Tailored Inhibitors. *Angewandte Chemie International Edition* **2021**, *60* (18), 10423-10429, https://doi.org/10.1002/anie.202016961. DOI: https://doi.org/10.1002/anie.202016961 (acccessed 2022/02/04). Brun, J.; Vasiljevic, S.; Gangadharan, B.; Hensen, M.; V. Chandran, A.; Hill, M. L.; Kiappes, J. L.; Dwek, R. A.; Alonzi, D. S.; Struwe, W. B.; et al. Assessing Antigen Structural Integrity through Glycosylation Analysis of the SARS-CoV-2 Viral Spike. *ACS Central Science* **2021**, *7* (4), 586-593. DOI: 10.1021/acscentsci.1c00058. Sanda, M.; Morrison, L.; Goldman, R. N- and O-Glycosylation of the SARS-CoV-2 Spike Protein. *Analytical Chemistry* **2021**, *93* (4), 2003-2009. DOI: 10.1021/acs.analchem.0c03173.

(21) Chang, V. T.; Crispin, M.; Aricescu, A. R.; Harvey, D. J.; Nettleship, J. E.; Fennelly, J. A.; Yu, C.; Boles, K. S.; Evans, E. J.; Stuart, D. I.; et al. Glycoprotein Structural Genomics: Solving the Glycosylation Problem. *Structure* **2007**, *15* (3), 267-273. DOI: https://doi.org/10.1016/j.str.2007.01.011.